Experimental Mechanics (2015) 55:1613–1625
DOI 10.1007/s11340-015-0050-0

Experimental Testing of Bend-Twist Coupled Composite Shafts

S.E. Rohde[1] · **P.G. Ifju**[1] · **B.V. Sankar**[1] · **D.A. Jenkins**[1]

Received: 9 January 2015 / Accepted: 3 June 2015 / Published online: 30 July 2015

Abstract Bend-twist coupling is a property of certain specially designed composite beams that when subjected to loading conditions that would normally result in pure bending, undergo both bending and twisting. This phenomenon is called bend-twist coupling. To fully characterize the degree of bend-twist coupling in the beam, shear center per unit length (e_y/L) must be determined. This paper proposes an experimental method for quantifying e_y/L. The specific method for manufacturing these composite shafts is detailed. A special apparatus was constructed to load the tip of a cantilever sample with an adjustable torque. Digital image correlation (DIC) was used to measure tip rotation and deflection. From these measurements shear center values were determined. Repeating this process for different shaft lengths and orientations allows for a final e_y/L measurement. Techniques are provided to reduce the various uncertainties in these measurements. The experiment utilizes three dimensional DIC, a rigid boundary condition such as a vice to simulate a cantilever condition, and an adjustable moment arm on which to load the specimen. The special case of a cylindrical carbon fiber beam is presented here, but the experimental methods can be generalized to tapered beams, non-circular cross-sections, and other orthotropic materials. The results are compared against finite element and analytical predictions. The final average experimental e_y/L for all four shafts is 8 % higher than what the analytical method and FEA predict.

Keywords Bend-twist coupling · Composite shaft · Extension-shear coupling · Shear center

Nomenclature

CF	Carbon fiber
COV	Coefficient of variation
CTE	Coefficient of thermal expansion
DIC	Digital image correlation
E_1	Young's modulus in the fiber direction
E_2	Young's modulus perpendicular to the fiber direction
e_y	Shear center along the horizontal y axis perpendicular to the shaft
FEA	Finite element analysis
L	Length of cantilever shaft free to rotate
S_{16}	Extension-shear coupling term defined as η/G
X	Parallel to shaft with the origin at the fixed end of the cantilever
Y	Horizontal to the shaft with the origin at the fixed end of the cantilever
Z	Vertical to the shaft with the origin at the fixed end of the cantilever
η	Coefficient of mutual influence

Introduction

First consider the more common case of an isotropic cantilevered beam. A transverse, eccentric load applied at the tip will cause the beam to bend in proportion to the load, and twist in proportion to the torque (load times moment arm). This property can be altered if the cross-section of the beam is changed to an asymmetric geometry. A classical example of this is a "C" channel beam as illustrated in Fig. 1 [1].

✉ S. E. Rohde
seanerohde@gmail.com

[1] Department of Mechanical and Aerospace Engineering, University of Florida, Gainesville, FL 32611, USA

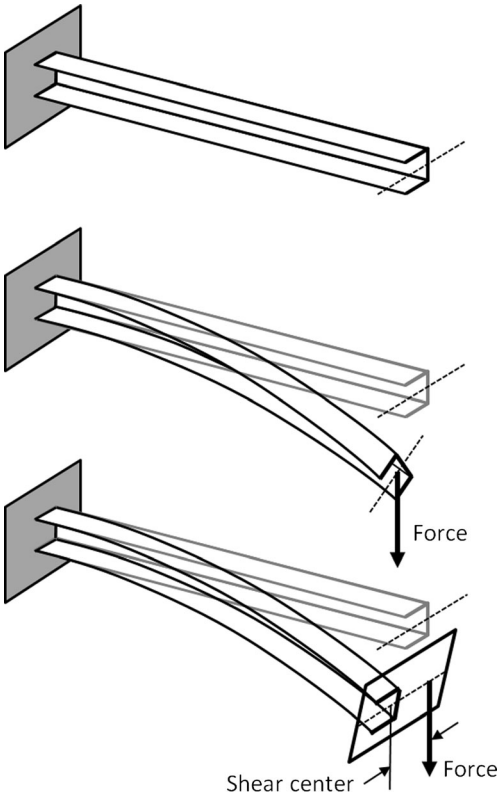

Fig. 1 Shear center resulting from shear flows in an isotropic beam with an asymmetric cross-section

Load applied at the tip's geometric centroid results in the beam twisting. This can appear counterintuitive the first time it is seen. A corollary to this is if a load is applied at the shear center, a certain distance from the centroid, the beam will not twist. In other words, the beam is being subjected to a torque that counteracts its natural tendency to twist. This location is called the shear center. It is the distance from the geometric centroid where a point load would not cause twisting. It defines the reference point from which all torque moment arms must be calculated to predict the degree of resulting twist.

In the vast majority of beams the material is isotropic and the cross-section's geometry is symmetric about both centroidal axes resulting in a shear center of zero (coincident with the centroid). Asymmetric beams such as the "C" channel with nonzero shear centers are said to possess bend-twist coupling. The causes of this isotropic bend-twist coupling are the unbalanced shear flows present in the cross-section which require the beam to twist in order to balance internal forces [1].

A second way to create bend-twist coupling is by orienting an orthotropic material asymmetrically. While the fundamental cause is different, the outward appearance of bend-twist coupling and an off-axis shear center remains the same. For this reason the terminology from the classical isotropic case is borrowed to interpret the anisotropic case presented here. Consider a cantilevered plate, shown in Fig. 2, consisting of orthotropic material that has greater stiffness along the fiber direction than the transverse direction.

The cause of the bend-twist coupling is not unbalanced cross-sectional shear flows but the extension-shear coupling resulting from the off-axis fiber orientation. Load tends to follow the path of greatest stiffness and, for an anisotropic material asymmetrically oriented, this results in shear strain for the bent plate. The half of the beam above the neutral axis experiences extension coupled with shear to the left. The other half of the beam below the neutral axis experiences compression coupled with shear to the right. With the top half shearing to the right and bottom half shearing to the left, the beam is experiencing shear equivalent to a counterclockwise rotation. The beam bends so it must twist. This property is reversible: pure torque applied to the beam will result in the beam bending. The plate geometry can be expanded about the neutral axis to hollow cross sections such as cylinders. This conceptual progression is shown in Fig. 3 with the fully realized example in Fig. 4. This cylindrical design is more similar to the bend-twist coupled composites studied previously [2, 3]. Much of the research in composite bend-twist coupling involves shapes such as wind turbine

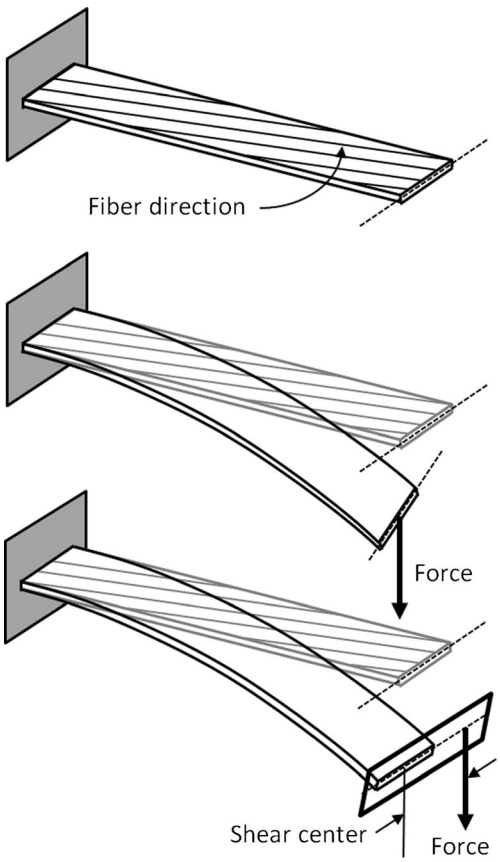

Fig. 2 Shear center resulting from bend-twist coupling in a composite beam with asymmetric fiber orientation

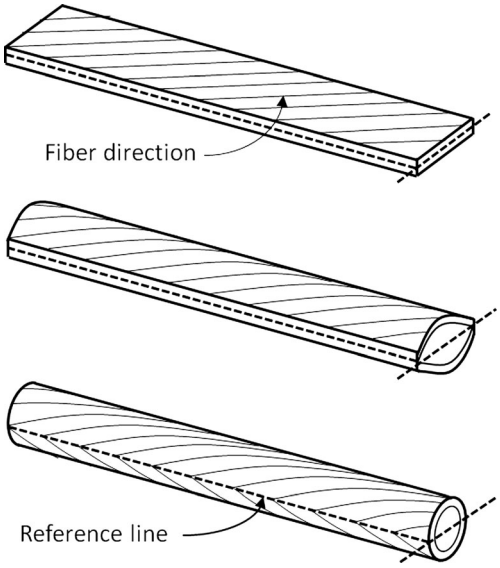

Fig. 3 Conceptual transition from plate to cylinder

blades [4, 5], marine propellers [6], and wings [7]. In these cases the goal is to align the shear center with the aerodynamic center. The property can also be used to prevent shear buckling [8]. Of particular concern here, is the potential application for composite shafts subjected to off axis loading such as golf clubs.

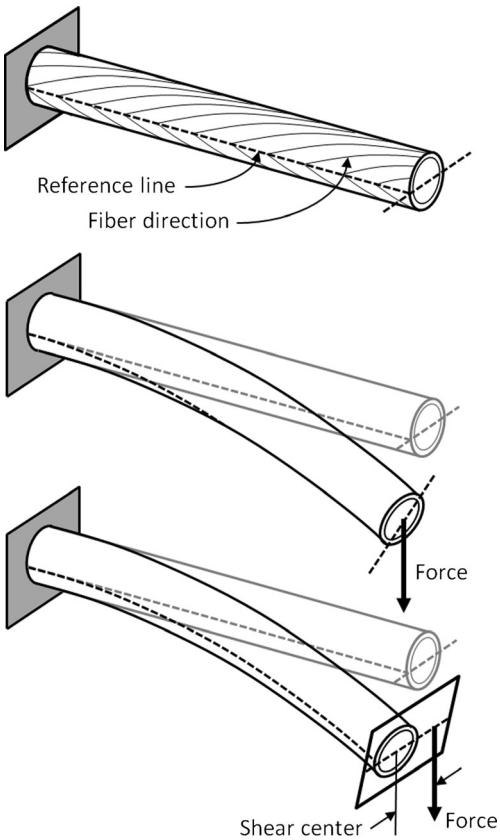

Fig. 4 Shear center resulting from extension-shear coupling in composite cylinder

Interpreting this effect using laminate plate theory, this property arises from a nonzero extension-shear coupling term (S_{16}). The coupling term is defined as

$$S_{16} = \frac{\eta_{16,1}}{G_{16}} \tag{1}$$

$$\begin{Bmatrix} \varepsilon_{11} \\ \varepsilon_{22} \\ \gamma_{12} \end{Bmatrix} = \begin{bmatrix} S_{11} & S_{12} & S_{16} \\ S_{12} & S_{22} & S_{26} \\ S_{16} & S_{26} & S_{66} \end{bmatrix} \begin{Bmatrix} \sigma_{11} \\ \sigma_{22} \\ \tau_{12} \end{Bmatrix} \tag{2}$$

The laminate is homogenized as an anisotropic material and uses equivalent elastic constants calculated from the original [A] matrix. Here, η is the coefficient of mutual influence. Figure 5 demonstrates how η varies as a function of the fiber direction relative to the beam axis [7–9].

Note that the more common case of symmetric ply angles (0° and 90°) results in an η of zero. This curve is unique for each composite material system. For every combination of material properties (E_1, E_2, G_{12}, etc.) there is an optimal lay-up that maximizes η and therefore the bend-twist coupling. This is typically between 18° and 23° for the carbon/epoxy material system used in this experiment.

Equation 2 makes it clear how shear strain can result in the absence of shear stress so long as the S_{16} term is present to multiply the longitudinal stress. In parallel research by Sankar et al. [10], this analytical work was developed further for the cylindrical case and results as a final equation for predicting the shear center for a given composite properties and orientations. Details of the derivation of equation 3 are presented in the Appendix section of this manuscript.

$$e_y = \frac{2\,\eta_{xs,x}\,L}{\pi\left(1 + \left(\frac{8}{\pi^2} - 1\right)\eta_{x,xs}\eta_{xs,x}\right)} \tag{3}$$

Where:

$$\frac{\eta_{xs,x}}{G_{xs}} = \frac{\eta_{x,xs}}{E_x} \tag{4}$$

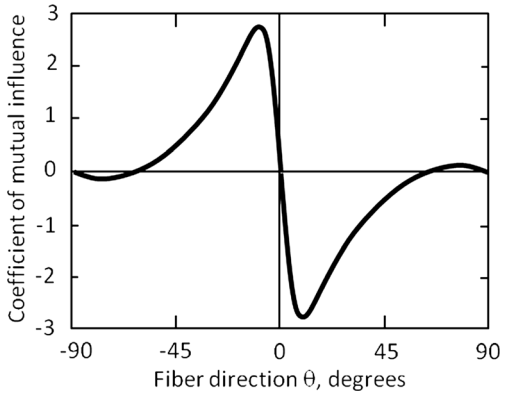

Fig. 5 η as a function of ply angle for carbon/epoxy [9]

In the above equation, what becomes apparent is that the shear center is now a function of beam length; it increases linearly with shaft length. This differs from the classical isotropic case where shear center was solely a cross-sectional property. This raises some interesting possibilities. A shear center of any length can be achieved if the beam is allowed to be long enough. Conversely, if the beam length is fixed, no amount of increasing the diameter will alter the shear center. The only way shear center can be altered is by changing the coupling coefficient η.

This dimensionless number, shear center per unit length, fully specifies the degree of bend-twist coupling achieved in a composite shaft. Any experimental method seeking to characterize the bend-twist coupling of a beam must concern itself with accurately estimating this value. The ratio e_y/L fully incorporates the unique combination of material properties and fiber orientations that define the shaft.

The experiment presented here utilizes DIC to measure tip deflections and rotations. Another method for locating the shear center of a beam is to measure the deflections with a pair of LVDTs. Point bending tests have also been applied for locating the shear center, called the torsional or elastic axis when referring to wings, on insect wings and other artificial wings [11, 12]. The advantage to using DIC for measuring tip deflections is that all three components of tip displacement u,v, w can be measured. DIC also makes possible direct measurement of both in-plane and out-of-plane rotation while maintaining sufficiently high resolution.

Presented here is a series of steps for experimentally determining e_y/L. Many of the steps were repeated multiple times in order to prevent uncertainty accumulating in the final e_y/L value. The results were then compared to values predicted by the analytical model given above and also with a finite element model [10]. Experimental validation of these models makes predictions possible. This is a necessary step in the optimization of bend-twist coupling for specific applications.

Experimental Procedures

Fabrication of Composite Shafts

The cylindrical composite shafts were constructed of four prepreg unidirectional carbon fiber layers with fiber orientations specified as $[0/23/23/0]_T$ as shown in Fig. 6. Each number designated the fiber orientation relative to the shaft axis. For example, a 0° layer consisted of the fibers oriented parallel to the shaft. While these 0° layers did not contribute to bend-twist coupling, they were added to increase flexural rigidity, prevent delamination, and lessen warping from residual strains. The inner and outer 0° layers were wrapped a full 360° around the shaft (plus a few extra degrees for overlap).

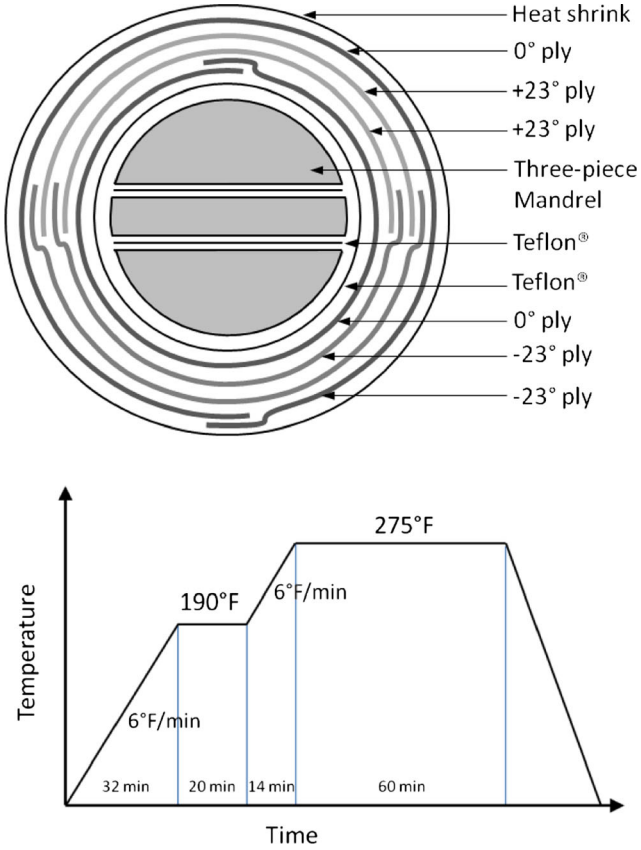

Fig. 6 Schematic of ply lay-up and curing cycle

The overlap was necessary to prevent delamination during the lay-up and curing as some thermal and chemical shrinkage occurs. The two middle 23° layers were responsible for the bend-twist coupling and were chevron patterns. They were called this because they appeared as chevrons when viewed from the side as shown in Fig. 4. This meant that +23° covered the top half of the cylinder and −23° covered the bottom half. They each wrapped 180° around the shaft with a few extra degrees of overlap. Through a combination of iterative progression, closed-form predictions, and FEA models the ideal chevron orientation for maximizing the degree of bend-twist coupling was determined to be between 18° and 23° for the carbon fiber used. For these reasons the lay-up $[0/23/23/0]_T$ was ideal for making simple shafts possessing both bend-twist coupling and structural integrity. The optimal angle of 23° was highly dependent on material properties E_1, E_2, and G_{12} making it necessary to know the precise elastic constants of the composite lamina. The manufacturer would not release the carbon fiber and matrix composition, so this testing was done in our lab. The curing cycle is shown in Fig. 6.

Because the majority of fibers lied in the longitudinal direction and the CTE of the epoxy matrix was much less than that of the carbon fiber, the curing process caused the laminate to grip the mandrel very tightly upon cooling. These compressive forces were so strong that all original attempts to extract

the cured shafts from the cylindrical mandrel resulted in the shafts fracturing.

To solve this problem a special mandrel was constructed to facilitate shaft extraction. The mandrel was 12.7 mm (1/2 in.) diameter and could be separated into three pieces longitudinally as in Fig. 7. This allowed for the gradual removal of the inner mandrel and then the inward collapse of the outer two.

The mandrel was constructed by soldering a sandwich of 9.5 mm (3/8 in.) by 25.4 mm (1 in.), 3.2 mm (1/8 in.) by 25.4 mm (1 in.), and 9.5 mm (3/8 in.) by 25.4 mm (1 in.) steel rectangular stock and then carefully turning them in a lathe until a single 12.7 mm (1/2 in.) diameter mandrel was formed. The tin solder was then melted out. The mandrel had a hole drilled through all three layers for a set screw to hold the layers in place. The middle 3.2 mm (1/8 in.) thick layer was kept longer with its own hole for extracting it. When the three layers were being combined, a thin sheet of Teflon® was added between each mandrel layer to reduce friction forces when it was time to remove them from the cured shaft. The mandrel was long enough to create shafts 469.9 mm (18.5 in.) in length. The longer the shaft, the less sensitive of e_y/L was to lengthwise manufacturing error, but the more difficult it was to machine the mandrel in a lathe.

The lay-up process began by combining the three mandrel pieces together in the order that they were turned and fixing them in place with the set screw. The outside of the mandrel was then wound in Teflon® to prevent the epoxy from adhering to the mandrel. The Teflon® must be tightly wound or epoxy seeps through the gaps of the Teflon®. The four layers of carbon fiber were cut out of the carbon fiber sheets. Two pieces were oriented in the 0° direction, and four half pieces were oriented at 23°. A protractor and straight edge were used for measuring the angles. Each successive layer was slightly larger to account for the increasing inner diameter as each layer was added. The layers were then wrapped around the mandrel. The interface at 180°, where the two 23° layers met, hold special significance. This tip of the chevron demarcated the reference line that, when oriented horizontally, produced the maximum shear center. The physics of this is explained in the Experimental Set-Up. For this reason it was clearly marked on the outside of the shaft in silver marker.

Fig. 7 The three pieces of the mandrel separated and combined

Two layers of plastic shrink wrap were then wound around the shaft to provide the compressive forces necessary for the carbon fiber to consolidate. After the heat cycle, Fig. 6, the shaft was removed from the mandrel by slowly extracting the middle layer of the three-piece mandrel. To gradually apply the axial force needed to remove the inner mandrel layer, a screw jack method was used to provide the necessary mechanical advantage. Once the inner layer was freed, the outer two layers collapsed inward and the carbon fiber shaft was easily removed.

Experimental Set-Up

The overall experimental set-up is shown in Figs. 8 and 9. Once the carbon fiber shaft was completed, a method was needed to load the beam's tip with an adjustable off-axis moment arm. This adjustable moment arm needed to maintain the same downward tip load but alter the amount of torque being applied. In this way the shear center was calculated as the moment arm length which resulted in zero tip rotation. To serve this function a special fixture was machined. The loading fixture, shown in Fig. 9, gripped the end of the shaft while a special block was free to slide horizontally. A constant weight was hung from this block to adjust the torque applied to the tip of the shaft.

To give the fixture something to grip to, a steel insert of 64 mm length and 13 mm diameter was adhered with epoxy into one end of the shaft so that 17 mm of excess steel insert exited the shaft. When recording the beam length during testing, it was important to subtract the length of the portion epoxied to the steel insert, as this portion was nearly rigid. After the loading fixture was added, a flat target was then adhered to the face of the steel insert. This flat target, Fig. 10, had been spray painted with a black speckle pattern and a white background. The average speckle size was on the order of 0.1 mm. The speckling was for providing the DIC system with a surface to measure tip displacement and rotation. The cross-sectional ends of the shaft were not required to be perfectly flat because they were free and unloaded.

The end of the shaft without the steel insert was clamped tightly in the vice to create the fixed end of the cantilevered beam. Two pieces of aluminum with a cylindrical core were

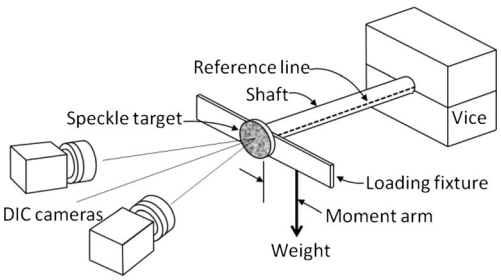

Fig. 8 Schematic of the experimental set-up

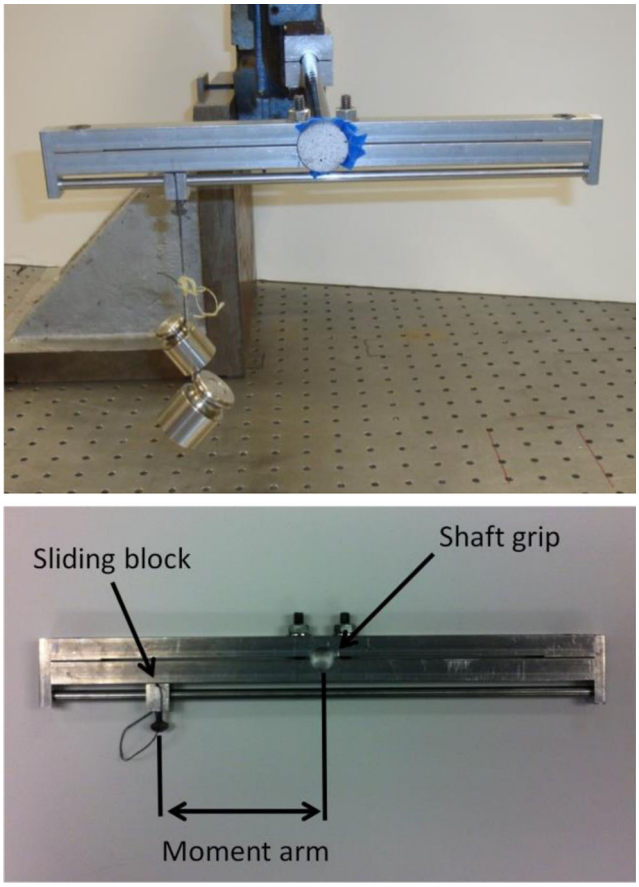

Fig. 9 Experimental set-up and loading fixture

machined to grip the contours of the shaft in the vice. Three inches of shaft were clamped to ensure a near fixed condition. The loading fixture was attached to the steel insert on the opposite end. The fixture was oriented as horizontal as possible using a level. A weight of 300 g was suspended from a string attached to the sliding block of the fixture. The weight was enough to clearly show tip deflection and rotation within the resolution of the DIC but not so large as to cause second order effects from excessive curvature. The camera's depth of focus was set accurately to capture the tip with and without the 300 g present.

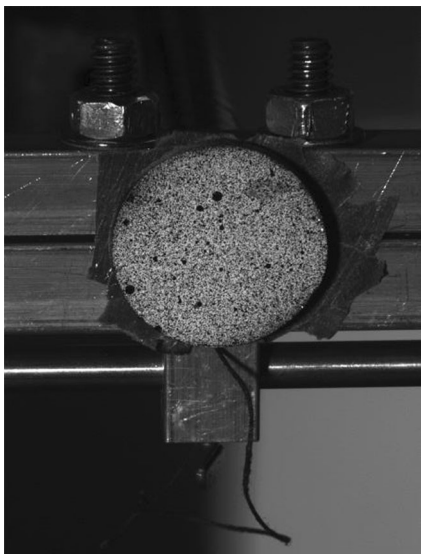

Fig. 10 Flat, speckled target for DIC

Table 1 Camera calibration

	Camera 1	Camera 2
Center x:	1158.78 pixel	1226.81 pixel
Center y:	976.05 pixel	1082.69 pixel
Focal length x:	11829.6 pixel	11954.9 pixel
Focal length y:	11829.1 pixel	11950.9 pixel
Skew:	−1.24791	1.44341
Kappa 1:	−0.232567	−0.294215
Kappa 2:	0	0
Kappa 3:	0	0

Next, the cameras in the DIC system were calibrated. A two-camera, 3D setup was needed because there were out-of-plane displacements. The specification of the camera was a Kreuznach Xenoplan CCD camera lens 1.9/35-0511. An LED flood light was placed behind the cameras to provide full and even lighting. The reference image was taken with the loading fixture present but the 300 g weight absent. Taking the reference image with the loading fixture present accounts for any bending and twisting that resulted from the fixtures own weight. Doing this did not alter the apparent location of the shear center. The principle of superposition allowed for this assumption and was valid within first order effects. The camera calibration results are shown in Tables 1 and 2.

Since tip rotation varied linearly as a function of moment arm for a constant load, a minimum of two points was needed to fully define that line. There was a very small amount of uncertainty in these measurements therefore, to accurately determine the shear center location, six different loading points were chosen giving six points to plot a best fit line. At each loading point DIC image pairs were taken. For these loading points the same 300 g weight was hung from six different evenly spaced positions of the sliding block. A caliper was used to measure each moment arm length. Care was taken to wait until all tip vibrations dampened before taking images.

Table 2 Camera transformation

Alpha:	0.549386°
Beta:	−51.0754°
Gamma:	−0.312273°
Tx:	212.651 mm
Ty:	0.306792 mm
Tz:	108.264 mm
Baseline:	238.624 mm

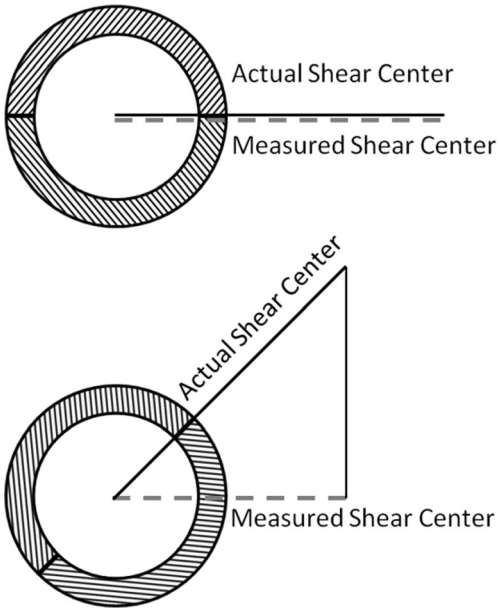

Fig. 11 Shear center's relation to this angle is defined by the cosine function

This set of six measurements produced one shear center value. Depending on how the reference line was oriented, the measured shear center would change. The reference line indicated the positioning for maximum shear center when oriented to the left or right. When facing upward or downward the shear center was zero as symmetry gives no reason for it to be otherwise. Figure 11 illustrates how this relationship is sinusoidal because the measured value is just the projection of the actual value onto the horizontal plane. Because of this, the measured shear center was highly sensitive to the orientation of the plane of symmetry with respect to the moment arm. There was a large risk that the reference line was not perfectly horizontal or even faithful to the underlying chevron pattern.

To correct for this uncertainty, eight shear centers were measured for eight evenly spaced global rotations. After each set of six images was taken, the shaft was rotated 45° and the loading fixture was realigned to be level with the ground. This eliminated the risk of not perfectly orienting the shaft to maximize the shear center. This set of eight was repeated at two different

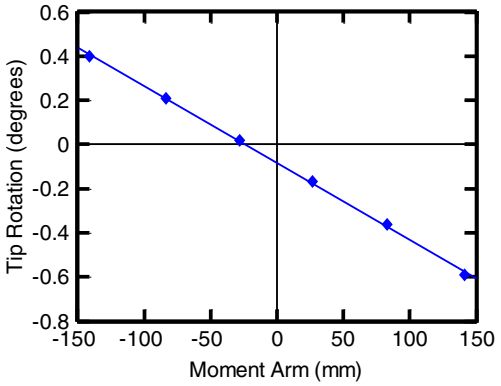

Fig. 13 Tip rotation as a function of moment arm. The average R^2 value was 0.999

beam lengths for each shaft. To reduce the beam length the shaft was slid farther into the vice before it was tightened.

It should be noted that since the sliding block was moved after the reference image was taken, it had a minor effect on the amount of apparent rotation of the shaft. This degree of distortion meant that the actual shear center was slightly larger than the apparent measured shear center in proportion to how much the sliding block weighed relative to the hanging mass. This came out to 1.8 %. All data were adjusted accordingly.

Post-processing

Two steps of post-processing were performed on the images taken during the experiment. The standard analysis used an image of the tip with the fixture but not the hanging weights as the reference image. The six images with a constant load but shifting moment arm were analyzed relative to this reference image to determine how the six different moment arms produced six different tip rotations. The tip rotations were derived using VIC Snap's in-plane rotation feature. Examples of the full-field displacements and in-plane rotations are shown in Fig. 12. The step and subset size were 5 and 42 pixels, respectively. These sizes were chosen using guidelines from the Correlated Solution user's manual and from experience that has shown these setting to be appropriate. Each of the six

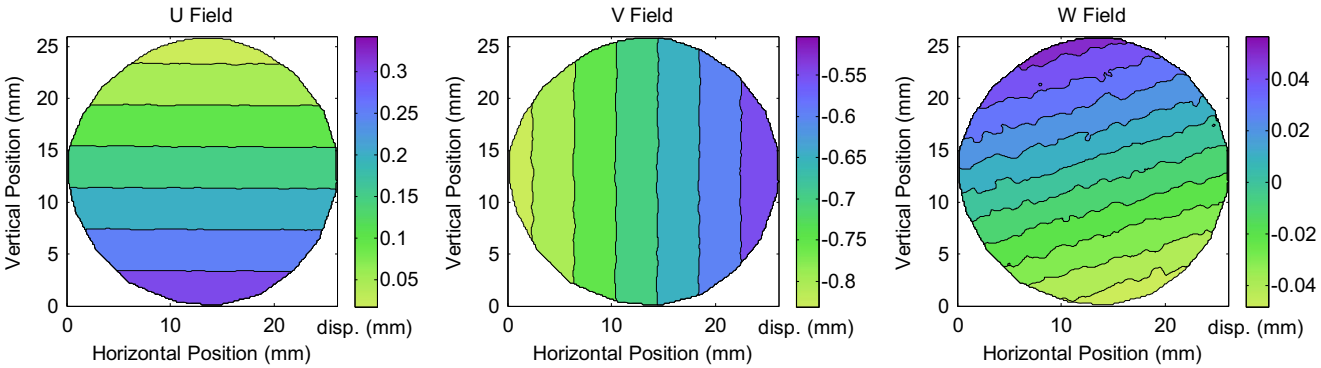

Fig. 12 Full field displacement of the flat target

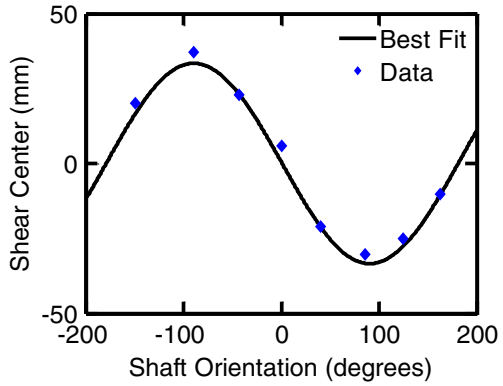

Fig. 14 A best fit sine wave with amplitude as the measure of bend-twist coupling

images taken had a moment arm value that was recorded using a caliper and a measure of tip rotation determined by DIC. This collection of six images was then plotted with tip rotation as a function of moment arm, an example being Fig. 13.

A best fit line was then produced using values from these six images. The shear center was the x-intercept of this line as the x-axis indicated zero degrees of rotation, the definition of shear center. The slope was a measure of the shaft's torsional rigidity. The R^2 value was recorded as a measure of accuracy. This process was repeated eight times, giving eight different shear center measurements for eight different shaft orientations at 45° intervals.

While nominally the shaft was rotated 45°, the exact value was important and could be determined using DIC. This was done using a second meta-analysis of the DIC images. This time all eight unloaded reference images were analyzed. One reference image was chosen to be the meta-reference image and the degrees of rotation were determined relative to this metric. The VIC-Snap software had difficulty processing these images because of the large 45° rotations and the incidental rigid body movements. To help the software perform, three reference points within the speckled target were manually selected for each image. The step and subset size were 5 and 32 pixels, respectively.

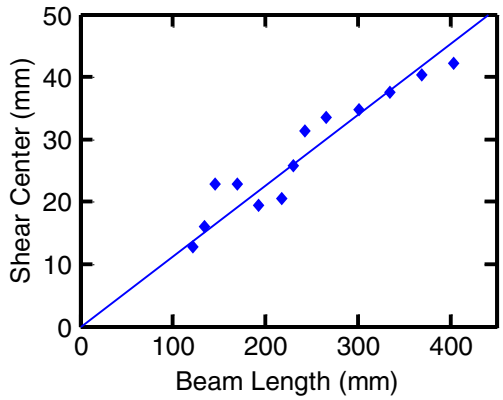

Fig. 15 Shear center as a function of beam length, $y=0.1153x$, $R^2=0.89$

Table 3 Sample A shear center values

Beam length (mm)	Shear center (mm)
121	13.0
134	16.2
145	23.3
169	23.2
192	19.7
218	20.8
230	26.3
243	31.9
266	34.1
301	35.4
335	38.2
369	41.1
403	43.0

Each set resulted in a different shear center that could be plotted along a sinusoid with shear center on the vertical axis and global shaft rotation on the horizontal axis. The shaft orientation values being precisely determined from the meta-analysis. The reason the curve was sinusoidal was because the measured shear center was the actual shear center projected onto the horizontal axis as previously shown in Fig. 11. Specifically, this was a negative sine function the way it was plotted and the angles were defined.

A sinusoidal curve was then fitted to the data points to minimize the sum of squared errors as in Fig. 14. The sine wave was allowed to phase shift up to 180° in either direction. This was done so that the original reference orientation did not matter. For the sake of experimental consistency, the reference image was always chosen with the reference line pointing upward. The sine wave had a period of 360° because the shaft had 360° of radial symmetry. The sine wave was centered about the x-axis (no parameter allowed any upward or downward shift) because there was no reason that the shear center should change whether loaded upward or downward. The equation is shown below. The variables A and φ are given free range with the goal of determining the pair of values that

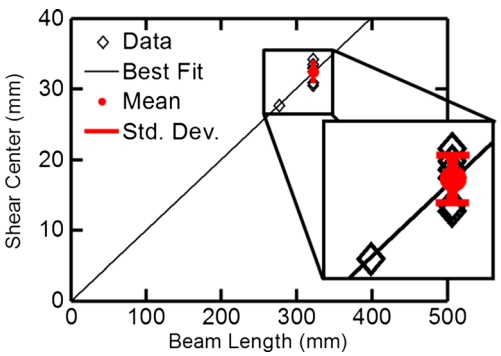

Fig. 16 One shaft repeated seven times at one location, mean=33.0 mm, std=1.3 mm

Table 4 Sample B shear center values

Beam length (mm)	Shear center (mm)
277	28.2
322	33.0
322	33.1
322	33.5
322	34.0
322	31.0
322	31.4
322	34.8

minimizes the sum of squared residuals between the best fit and the eight data points.

$$Y = -A\sin(\theta + \varphi) \tag{5}$$

The amplitude of the sine wave was the second parameter that was allowed to change freely. The amplitude represented the maximum shear center that could be obtained when the shaft was oriented with the reference line perfectly horizontal. It was this value that defined the shear center for this beam length.

Shear center amplitude was a linear function of the length of the beam. For this experiment, the shear center amplitude was calculated at multiple beam lengths. A graph was then made with shear center on the vertical axis and beam length on the horizontal axis. A best fit line was then plotted through the origin and the two shear center values. The slope of this line, shear center per unit beam length, was the defining characteristic of each beam that fully defined its bend-twist coupling. The experiment was designed to minimize the uncertainty in this final value given available resources.

To measure the uncertainty in the manufacturing process, these series of tests were performed on four different shafts. Nominally the shafts had the same design. Two of the shafts had extra tests performed. One shaft was specially tested to measure variance in e_y/L along beam length. The second shaft was repeatedly tested at the same beam length to quantify uncertainty in the measurement of shear center.

Results

The first series of tests were designed to examine how shear center varies as a function of beam length. The same shaft was tested to find the shear center for 13 different beam lengths.

Table 5 Sample C shear center values

Beam length (mm)	Shear center (mm)
277	26.7
322	36.0

Table 6 Sample D shear center values

Beam length (mm)	Shear center (mm)
277	16.5
322	27.1

The 13 different lengths for a single shaft were achieved by sliding the shaft farther into the vice so that the length of the shaft acting as a cantilever beam changed. Each point represents the amplitude of a fitted sine wave for that beam length. The results are shown in Fig. 15 and detailed in Table 3. The prediction that shear center would increase linearly as a function of length is verified. The shear center increases on average 0.12 mm for every 1 mm of added beam length.

The variance between data points and fit is 11 % and represents a combination of measurement uncertainty and lengthwise uncertainty. Much of the lengthwise uncertainty is in the manufacturing step. Manufacturing errors result in an underlying variance in the degree of bend-twist coupling, η, which is averaged out as the measured beam length increases, like regression to the mean. This explains why the variance is greatest when the beam is shortest and then decreases as the beam elongates; it is being averaged out. During the lay-up, carbon fiber strips are wrapped around the mandrel to form chevrons. Ideally each region covers exactly 180° and does not shift lengthwise along the mandrel. In practice there are several degrees of variance as the layers are added. This large sensitivity to ply angle agrees with the results of the sensitivity test discussed below. This is why shafts of this length have been chosen, as it is sufficiently long to diminish these effects, but still short enough to fit on a well turned mandrel.

The next series of tests were designed to isolate the uncertainty in the measurement of shear center. A second shaft was tested repeatedly at a constant beam length. Each time the series of eight sets were performed to determine the shear center amplitude at a constant beam length of 323 mm. A second point was tested at 277 mm. The seven identical tests resulted in a mean shear center of 33.0 mm with a standard of deviation of 1.3 mm (COV of 4 %). The graph in Fig. 16 includes the standard of deviation to help illustrate the measurement uncertainty. This 4 % COV, while not perfect, is much lower than the 11 % in Fig. 15 which resulted from both manufacturing and measurement uncertainty. The values are detailed in Table 4.

Table 7 Average shear center per unit length for each shaft tested

Sample	Shear center per unit length (mm/mm)
A	0.119
B	0.102
C	0.104
D	0.072

Two more shafts were tested at 277 and 322 mm to observe the amount of variance across separate shafts. The shafts nominally have the same dimensions, but manufacturing errors can result in different shear centers to an extent greater than that observed lengthwise along the same shaft. These final values represent the cumulative uncertainty of measurement, length, and shaft variance. The average across the four shafts was an e_y/L of 0.099 with a standard of deviation of 0.018 giving a COV of 18 %.

The average shear center value summarizes the results of the 25 sets of experiments performed. These experiments are detailed in Tables 3, 4, 5, and 6 with individual shaft averages in Table 7. The goal of performing multiple experiments is to average out as much uncertainty as possible. The overall shear center value, e_y/L=0.099, is then compared to the predictions made by the analytical expression given in equation 3 and FEA.

A finite element analysis was performed using the commercial software Abaqus using quadrilateral shell elements with eight nodes per element, Fig. 17. Each node had six degrees of freedom. Nominal element size was 1.7×3.5 mm, and the number of elements varied from 830 to 2760 depending on the shaft length. There were 24 elements in the circumferential direction. Shell elements were chosen because the shaft thickness was small compared to the radius (r/t=9.9). The elastic constants used were based on testing performed on the carbon fiber epoxy laminate in our laboratory. Three simple laminates were tested in various loading directions. The material properties were determined to be: E_1=81.0 GPa, E_2=5.45 GPa, G_{12}=3.0 GPa, G_{13}=3.0 GPa G_{23}=2.0 GPa, ν_{12} =0.3, and ply thickness=0.16 mm. These were the same values used in the analytical solution. The results are shown in Table 8. The agreement between the analytical method and FEA was nearly exact. The experimental results showed an e_y/L 8 % higher than predicted.

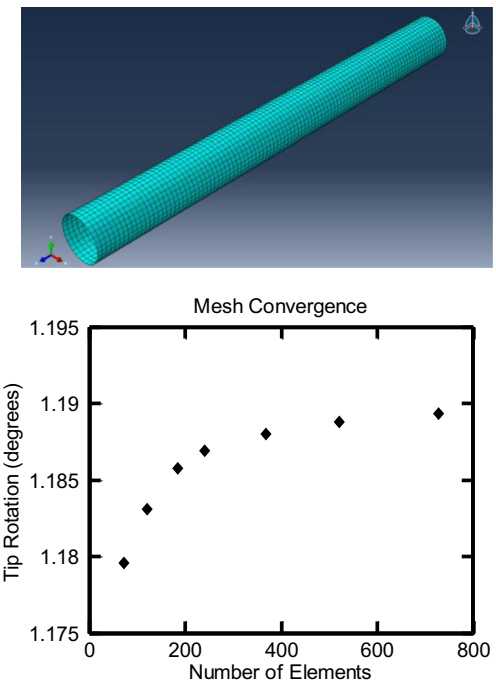

Fig. 17 FEA model of shaft and mesh convergence

Table 8 Comparison of techniques

Sample	Shear center per unit length (mm/mm)
Experimental	0.099
Analytical	0.092
FEA	0.092

The most likely cause for exceeding the predicted e_y/L value is that the three inches of shaft clamped in the vice are twisting, thus not an ideal clamped cantilever condition. The analytical and FEA models assume that the shaft completely stops twisting at the boundary. In reality some twisting continues into the clamped portion due to finite friction forces. This effectively lengthens the portion of the beam free to twist by zero to three inches. This would increase the experimental e_y/L value in proportion to how much it increases the effective beam length. This is consistent with exceeding the analytical and FEA predictions.

Using the analytical prediction of shear center, a sensitivity test was performed to measure the relative importance of each input on the determination of shear center. Shown in Fig. 18, the results indicate obtaining an accurate ply angle was the most important step. The second most critical value was the shear modulus G_{12}, with E_2 in third. Ply thickness did not affect shear center in this analysis because each layer had the same thickness and the cylinder was assumed to have negligible thickness as compared to the radius (r/t=9.9). The ply angle θ 's effect on shear center was asymmetric because θ moves the value of η along the curve in Fig. 5. This shows that extra resources and effort should be directed towards guarantying that the physical ply angles match the desired nominal angles, and that G_{12} and E_2 are known to the greatest possible accuracy. Not shown here was the sensitivity to beam

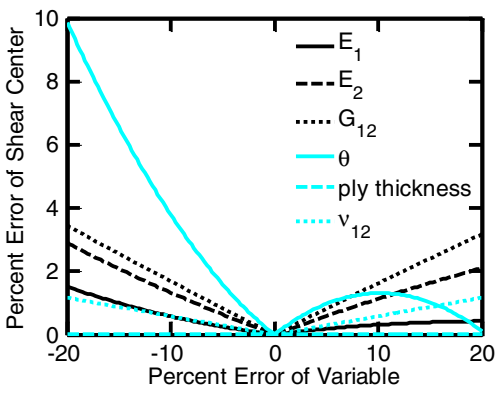

Fig. 18 Relative effect each material property had on shear center

length which would be a one to one ratio, by far the most sensitive parameter. The beam length was the measured portion of the shaft not gripped in the vice and not adhered to the steel insert i.e., the length of shaft free to twist. In reality there may have been some twisting of the shaft in the vice, while the analytical and FEA models assume absolute rigidity at this boundary region. This made the effective beam length longer than what had been recorded and would lower the experimental e_y/L. This would bring greater agreement with the predictions.

Conclusion

A series of techniques was presented for experimentally locating the shear center of a composite shaft with a novel set up. A dimensionless number for the shear center per distance unit length was calculated. This value fully quantified the degree of bend-twist coupling in the shaft. The experimental steps were repeated multiple times in order to minimize the uncertainty present at that step. Currently, there is 4 % variance in the measurement of shear center, 7 % variance in shear center along the length, and 6 % variance in e_y/L across separate shafts. The final average e_y/L for all four shafts is 8 % higher than what the analytical method and FEA predict. Part of this 8 % difference arises due to the uncertainty in the construction of shafts themselves implying more numbers should be tested. Agreement with the predictive model is sufficiently close to begin with using the model for design and optimization. If greater experimental accuracy is needed there should be more data points to be tested along the length of each shaft and a larger number of shafts to be constructed and tested. If greater model fidelity is needed there should be more thorough testing of G_{12}, E_2, and the effective beam length. The shafts were able to achieve shear centers one tenth of their length ($e_y/L=0.099$), despite having only half the plies oriented at 23° to contribute to bend-twist coupling. Shear center per length values greater than this should be achievable.

Appendix

Consider a thin-walled tube with the tube axis parallel to the x-axis. The mean radius of the tube is R and the wall thickness $h<<R$. The tube is made of two anisotropic materials - top half ($0<\theta<\pi$) is made of Material 1 and the bottom half ($\pi<\theta<2\pi$) is of Material 2. We assume that the tube is in a state of plane stress normal to the radial direction n, see Fig. 19, such that $\sigma_{nn}=\tau_{nx}=\tau_{ns}=0$. Furthermore, we assume the hoop or circumferential stress $\sigma_{ss}=0$. Thus the two significant stresses are the axial stress σ_{xx} and the shear stress τ_{xs}. We assume that the tube deforms such that plane sections remain plane and

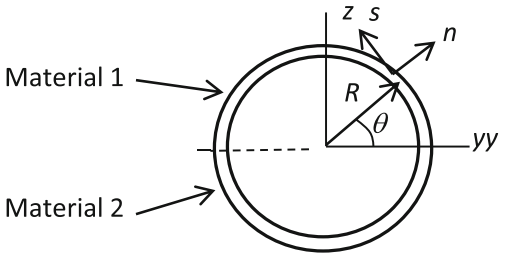

Fig. 19 Cross section of the tube and the coordinate system

normal to the tube axis as in Bernoulli-Euler beam theory. Then the displacement field can be written as

$$\begin{aligned} u(x,y,z) &= u_0(x) - y\frac{dv_0}{dx} - z\frac{dw_0}{dx} \\ v(x,y,z) &= v_0(x) \\ w(x,y,z) &= w_0(x) \end{aligned} \tag{6}$$

where u_0, v_0 and w_0 are the deflections of the beam axis. The axial strain takes the form

$$\begin{aligned} \varepsilon_{xx} &= \frac{\partial u}{\partial x} \\ &= \frac{\partial u_0}{\partial x} - y\frac{d^2v_0}{dx^2} - z\frac{d^2w_0}{dx^2} \\ &= \varepsilon_{xo} + y\kappa_y + z\kappa_z \end{aligned} \tag{7}$$

where κ_y and κ_z are the curvatures. But we assume the shear stress is uniform and given by

$$\tau_{xs} = \frac{T}{2\pi R^2 h} = \tau_0 \tag{8}$$

where T is the torque acting on a cross section.

The constitutive relation for both materials can be written in the form [13]

$$\begin{Bmatrix} \varepsilon_{xx} \\ \gamma_{xs} \end{Bmatrix} = \begin{bmatrix} \frac{1}{E_x} & \frac{\eta_{xs,x}}{G_{xs}} \\ \frac{\eta_{x,xs}}{E_x} & \frac{1}{G_{xs}} \end{bmatrix} \begin{Bmatrix} \sigma_{xx} \\ \tau_{xs} \end{Bmatrix} = \begin{bmatrix} \overline{S}_{11} & \overline{S}_{16} \\ \overline{S}_{16} & \overline{S}_{66} \end{bmatrix} \begin{Bmatrix} \sigma_{xx} \\ \tau_{xs} \end{Bmatrix} \tag{9}$$

Then from (2), (3) and (4) we obtain

$$\begin{aligned} \sigma_{xx} &= E_x\varepsilon_{xx} - \eta_{x,xs}\tau_{xs} \\ &= E_x\left(\varepsilon_{x0} + y\kappa_y + z\kappa_z\right) - \eta_{x.xs}\tau_0 \end{aligned} \tag{10}$$

The force and bending moment resultants are defined as

$$\begin{aligned} \left(P, M_y, M_z\right) &= \int_A \sigma_{xx}\ (1, z, -y)dA \\ &= \int_0^{2\pi} \sigma_{xx}(1, R\sin\theta, -R\cos\theta)Rhd\theta \end{aligned} \tag{11}$$

where the integration is performed over the cross section of the tube.

Performing the integration we obtain relations between the force and moment resultants and deformations:

$$\begin{bmatrix} \overline{E}_x A & \frac{AR}{\pi}\Delta E_x \\ \frac{AR}{\pi}\Delta E_x & \overline{E}_x I \end{bmatrix} \begin{Bmatrix} \varepsilon_{x0} \\ \kappa_z \end{Bmatrix} = \begin{Bmatrix} P \\ M_y \end{Bmatrix} + \begin{Bmatrix} A\overline{\eta}_{x,xs} \\ 2R^2 h\,\Delta\eta_{x,xs} \end{Bmatrix} \tau_0$$
$$\overline{E}_x I \kappa_y = -M_z \tag{12}$$

The average torsional rotation ψ_x is calculated as follows. Let us define the average unit angle of twist $\overline{\phi} = d\psi_x/dx$. The shear strain can be written as

$$\gamma_{xs} = R\phi + \frac{1}{R}\frac{\partial u}{\partial \theta} \tag{13}$$

Then the average unit angle of twist is obtained as

$$\begin{aligned} \overline{\phi} &= \frac{1}{2\pi}\int_0^{2\pi} \phi\, d\theta \\ &= \frac{1}{2\pi}\int_0^{2\pi} \frac{\gamma_{xs}}{R} d\theta - \frac{1}{2\pi}\int_0^{2\pi} \frac{1}{R^2}\frac{\partial u}{\partial \theta} d\theta \\ &= \frac{1}{2\pi R}\int_0^{2\pi} \gamma_{xs}\, d\,\theta \end{aligned} \tag{14}$$

From the constitutive relation (4) the shear strain at a point on the circumference of the tube can be written as

$$\gamma_{xs} = \frac{\eta_{x,xs}}{E_x}\sigma_{xx} + \frac{\tau_{xs}}{G_{xs}} \tag{15}$$

Substituting for σ_{xx} from (5) into (10) and then substituting for γ_{xs} from (10) into (9) the average unit angle of twist can be derived as

$$\overline{\phi} = \frac{\overline{\eta}_{x,xs}}{R}\varepsilon_{x0} + \frac{\Delta\eta_{x,xs}}{\pi}\kappa_z + \frac{1}{R}\left[-\overline{\left(\frac{\eta_{x,xs}^2}{E_x}\right)} + \frac{1}{\overline{G}_{xs}}\right]\tau_0 \tag{16}$$

where

$$\overline{\left(\frac{\eta_{x,xs}^2}{E_x}\right)} = \frac{1}{2}\left(\frac{\left(\eta_{x,xs}^{(1)}\right)^2}{E_x^{(1)}} + \frac{\left(\eta_{x,xs}^{(2)}\right)^2}{E_x^{(2)}}\right)$$
$$\frac{1}{\overline{G}_{xs}} = \frac{1}{2}\left(\frac{1}{G_{xs}^{(1)}} + \frac{1}{G_{xs}^{(2)}}\right) \tag{17}$$

It is assumed $+\alpha$ for the top half of the tube (Material 1) and $-\alpha$ for the bottom half (Material 2).

Then equations (12) and (16) can be simplified as

$$\begin{aligned} &\overline{E}_x A\varepsilon_{x0} = P \\ &\overline{E}_x I\kappa_z = M_y + 4R^2 h\,\eta_{x,xs}^{(1)}\tau_0 \\ &\overline{E}_x I\kappa_y = -M_z \\ &\overline{\phi} = \frac{2\eta_{x,xs}^{(1)}}{\pi}\kappa_z + \frac{1}{R}\left[\frac{1}{\overline{G}_{xs}} - \frac{\left(\eta_{x,xs}^{(1)}\right)^2}{\overline{E}_x}\right]\tau_0 \end{aligned} \tag{18}$$

From the above relations (2nd and 4th equations) one can note the coupling between the bending moment M_y and the torque T. The two relevant equations can be written as

$$\begin{aligned} \kappa_z &= \frac{M_y}{\overline{E}_x I} + \frac{2\eta_{x,xs}^{(1)}}{\pi\overline{E}_x I} T \\ \overline{\phi} &= \frac{4\eta_{xs,x}^{(1)}}{\pi\overline{G}_{xs}J} M_y + \left(1 + \left(\frac{8}{\pi^2} - 1\right)\eta_{x,xs}^{(1)}\eta_{xs,x}^{(1)}\right)\frac{T}{\overline{G}_{xs}J} \end{aligned} \tag{19}$$

In deriving the above relations we have used $T=2\pi R^2 h\tau_0$, $J=2I=2\pi R^3 h$, and the symmetry relation $\eta_{x,xs}/E_x=\eta_{xs,x}/G_{xs}$.

Consider a cantilevered tube clamped at $x=0$. First we will consider the case where the tube is subjected to a force F_z at the tip $x=L$. The force is such that the line of action is through the center of the tube. The bending moment distribution is given by $M_y(x)=-F_z(L-x)$. The tip rotation about the x-axis can be obtained from the second of equation (14):

$$\frac{d\psi_x}{dx} = \overline{\phi} = \frac{4\eta_{xs,x}^{(1)}}{\pi\overline{G}_{xs}J} F_z(x-L) \tag{20}$$

Integrating the above equation and noting $\psi_x(0)=0$ we obtain the tip rotation ψ_x^F due the transverse force F_z as

$$\psi_x^F = \frac{-2\eta_{xs,x}^{(1)}}{\pi\overline{G}_{xs}J} F_z L^2 \tag{21}$$

From (14) the rotation ψ_x^T due to torque T can be derived as

$$\psi_x^T = \left(1 + \left(\frac{8}{\pi^2} - 1\right)\eta_{x,xs}^{(1)}\eta_{xs,x}^{(1)}\right)\frac{TL}{\overline{G}_{xs}J} \tag{22}$$

The location of the shear center can be derived as follows. Let the shear center distance – distance of the shear center from the tube axis – be denoted by e_y. That is, if the transverse force F_z is applied at the shear center it would not produce any twisting of the tube, as the torque produced by the eccentric loading, $F_z e_y$, would cause an angle of twist equal in magnitude but opposite in direction to that produced by the force F_z. Then,

$$\psi_x^F = -\frac{\psi_x^T}{T}\left(F_z e_y\right) \Rightarrow e_y = \frac{-\left(\psi_x^F \big/ F_z\right)}{\left(\psi_x^T \big/ T\right)} \tag{23}$$

Substituting from (16) and (17) in the above equation, the shear center distance can be written in a non-dimensional form as

$$\frac{e_y}{L} = \frac{-\left(\psi_x^F \Big/ F_z\right)}{\left(\psi_x^T \Big/ T\right)L} = \frac{2\eta_{xs,x}^{(1)}}{\pi\left(1 + \left(\frac{8}{\pi^2} - 1\right)\eta_{x,xs}^{(1)}\eta_{xs,x}^{(1)}\right)} \tag{24}$$

From (13) we note that the bending moment M_z due to a transverse force F_y will not cause any twisting. Hence the shear center will be on the y-axis at a distance e_y from the center of the tube.

References

1. Timoshenko SP (1945) Theory of bending, torsion and buckling of thin-walled members of open cross section. J Franklin Inst 239(4): 249–268
2. Rehfield LW (2001) A refined simple model for tailoring box beams with composites. In Proceedings of the 42nd AIAA/ASME/ASCE/AHS/ASC Structures, Structural Dynamics, and Materials Conference, Seattle, WA, USA, AIAA Paper (Vol. 1333, p. 2001)
3. Raither W, Bergamini A, Ermanni P (2012) Profile beams with adaptive bending–twist coupling by adjustable shear centre location. J Intell Mater Syst Struct. doi:10.1177/1045389X12458040
4. Jureczko M, Pawlak M, Mężyk A (2005) Optimisation of wind turbine blades. J Mater Process Technol 167(2):463–471
5. Malcolm DJ, Laird DL (2007) Extraction of equivalent beam properties from blade models. Wind Energy 10(2):135–157
6. Liu Z, Young YL (2009) Utilization of bend–twist coupling for performance enhancement of composite marine propellers. J Fluids Struct 25(6):1102–1116
7. Kosmatka JB (1992) Extension-bend-twist coupling behavior of nonhomogeneous anisotropic beams with initial twist. AIAA J 30(2):519–527
8. Loughlan J (2001) The shear buckling behaviour of thin composite plates with particular reference to the effects of bend–twist coupling. Int J Mech Sci 43(3):771–792
9. Hyer MW (2009) Stress analysis of fiber-reinforced composite materials. DEStech Publications, Inc
10. Jonnalagadda A, Savant A, Rohde SE, Sankar BV, Ifju PG (forthcoming) An analytical model for composite tubes with bend-twist coupling. Composite Structures
11. Ha NS (2012) Static and dynamic characteristics of an artificial wing mimicking an Allolmyrina Sichotoma beetle's hind wing for flapping-wing micro air vehicles. Exp Mech 52:1535–1549
12. Ganguli R (2010) An experimental and numerical study of Calliphora wing structure. Exp Mech 50:1183–1197
13. Gibson RF (2012) Principles of composite material mechanics. CRC Press